Landau-level crossing in two-subband systems in a tilted magnetic field

C. A. Duarte, G. M. Gusev, A. A. Quivy, T. E. Lamas, and A. K. Bakarov*
Instituto de Física da Universidade de São Paulo, Caixa Postal 66318, CEP 05315-970 São Paulo, São Paulo, Brazil

J. C. Portal
GHMFL-CNRS, Boîte Postale 166, F-38042 Grenoble Cedex 9, France;
INSA-Toulouse, 31077 Cedex 4, France;
and Institut Universitaire de France, Toulouse, France

(Received 6 October 2006; revised manuscript received 25 May 2007; published 28 August 2007)

We have studied the quantum Hall effect in parabolic $Al_xGa_{1-x}As$ and square GaAs quantum wells with two occupied subbands in magnetic fields B tilted by an angle Θ with respect to the normal to the sample. We built the density–magnetic field n_s-B and angle-magnetic field Θ-B topological diagrams for the longitudinal resistivity ρ_{xx} and observed that the latter shows a similarity with a simulation based on a single-particle harmonic potential approximation.

DOI: 10.1103/PhysRevB.76.075346 PACS number(s): 73.43.Qt, 73.63.Hs

I. INTRODUCTION

Recently, the study of the quantum Hall effect in two-subband electron systems has attracted attention because of the interest on the study of the regime of Landau-level crossing between different subband energies. Numerous theoretical models based on Hartree-Fock calculations predict different symmetry breaking ground states in quantum Hall effect systems, when two Landau levels become degenerate near the Fermi level, among which quantum Hall ferromagnetism (QHF) is rather intriguing and well developed.[1] In single quantum wells with two subbands or in bilayer systems, quantum Hall ferromagnetism is described in terms of the pseudospin, which consists of real spin, orbit radius quantum number, and subband or layer index of the involved Landau levels.[2] The quantum Hall ferromagnet occurs when the pseudospin of the Landau level is completely aligned. When two Landau levels are nearly degenerated, the pseudospin orientation is determined by the minimization of the Hartree-Fock ground-state energy, and a ferromagnetic phase transition should be observed at the crossing point. Therefore, the coincidence of Landau levels allows us to study ferromagnetic phase transitions by varying the many external parameters.

Figure 1 demonstrates the Landau fan diagram for a system with two occupied subbands and six lowest spin splitted Landau levels for each subband. We label a set of quantum numbers (i,N,σ), where $i=0,1$; $N=0,1,\ldots$, and $\sigma=\uparrow,\downarrow$ correspond to the subband, Landau orbital, and spin indices. In the figure, the crossing of levels $(1,0,\downarrow)$ and $(1,0,\uparrow)$ with levels $(0,2,\downarrow)$ and $(0,2,\uparrow)$ is indicated by the dashed circle. The crossing of these levels encloses a diamondlike structure, shown in detail in Fig. 2(a). Figure 2(b) shows the calculated density–magnetic field n_s-B topological diagram for the longitudinal resistivity ρ_{xx} (details of the calculations are shown in Sec. II), which is very different from the energy–magnetic field diagram from Fig. 2(a). Recently, such topological diagram was studied in a square single quantum well with two occupied subbands[3] and was denominated as a "ringlike structure." It has been argued that such ring structure cannot be explained by noninteracting models, and collective states would be needed to describe the ground state in the level-crossing regime, likely connected with ferromagnetic order. In a previous study,[5] the n_s-B diagram clearly demonstrated a set of rectangular structures connected to Landau-level crossings with different pseudospins. It was shown that the ringlike structure in the topological n_s-B phase diagram corresponds to the crossing of Landau levels, while the intersubband anticrossing effect due to the ferromagnetic phase transition results in the squarelike structure in the same phase diagram.[4] It is not clear yet why the correlation effects in the samples may lead to a ferromagnetic transition or perfect subband locking effect. From the other side, it was shown that a single-particle model is sufficient to explain the vanishing magnetoresistance and the appearance of peaks in terms of the nonmonotonic behavior of the Fermi energy at the Landau-level crossing points.[6] Additional arguments are necessary to understand the nature of the Landau-level coincidence in the quantum Hall effect regime.

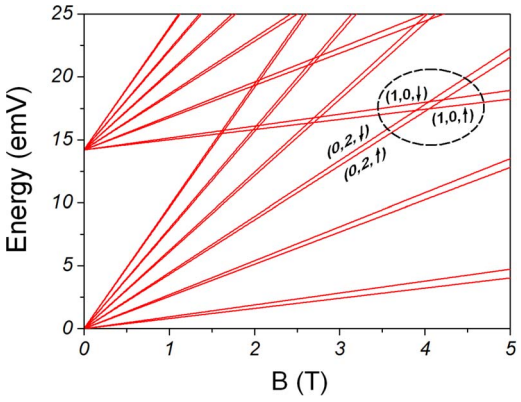

FIG. 1. (Color online) Landau fan diagram for a two-subband system with a subband energy separation of 14.2 meV. We show only the lowest six Landau levels and they are spin splitted. The encircled region marks a particular crossing of levels that we will refer to later.

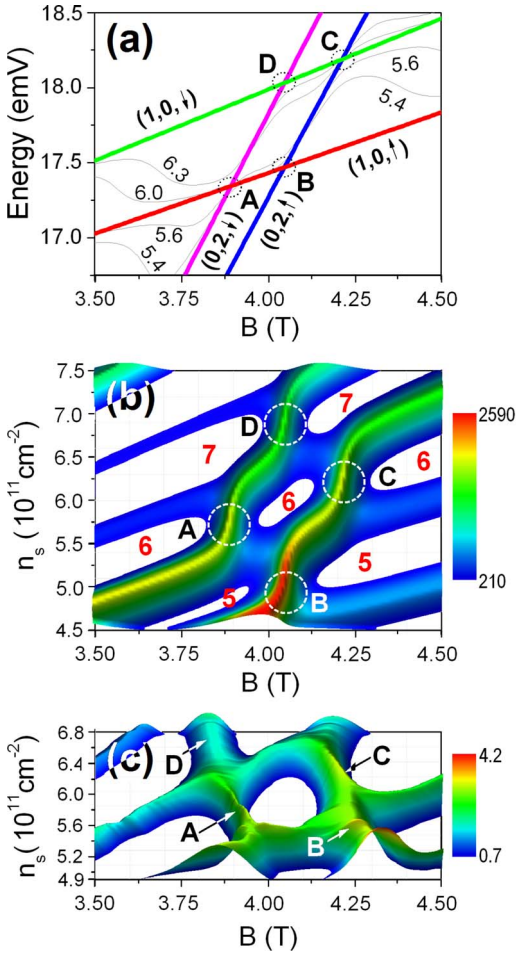

FIG. 2. (Color online) (a) Details of the Landau fan presented in Fig. 1. The labels in the figure are explained in the text. (b) Corresponding calculated magnetoresistance in the n_s-B plane. Filling factors measured from the Hall resistance are labeled. The meaning of labels A, B, C, and D are explained in the text. (c) Experimentally determined plot of the longitudinal resistivity at $T=50$ mK for a 500 Å $Al_xGa_{1-x}As$ parabolic well.

It is worth noting that the Landau-level crossing (anticrossing) is observed not only in the n_s-B phase diagram in a perpendicular magnetic field but also in the presence of a tilted magnetic field[7] for a fixed electron density.

In the present paper, we extend the study of the intersubband Landau-level crossing to different quantum structures (square and parabolic wells) and different types of topological diagrams.

II. EXPERIMENTAL RESULTS IN A PERPENDICULAR MAGNETIC FIELD

Here, we investigate two different systems (parabolic quantum well and square well) with high mobilities in order to analyze the Landau-level (LL) crossing in a perpendicular magnetic field. Table I shows the summary of the sample parameters. The $Al_xGa_{1-x}As$ parabolic wells can be characterized by the effective bulk density, which is given by the equation $n_+=\frac{\Omega_0^2 m^* \varepsilon}{4\pi e^2}$, where m^* is the effective mass and $\Omega_0=(2a/m^*)^{1/2}$ is associated to the conduction-band parabolic potential $V(z)=az^2$. The effective thickness of the electronic slab in parabolic wells can be obtained from the equation $W_{\text{eff}}=n_s/n_+$, where n_s is the two-dimensional density. In square GaAs quantum wells, the width W_{eff} has the same value as the bare quantum well width W. The test samples were Hall bars with the distance between the voltage probes $L=200$ μm and the width of the bar $d=100$ μm. The carrier density was varied by applying a gate voltage. We measured the longitudinal and Hall resistivities for different gate voltages (positive and negative) at $T=50$ mK, 300 mK, and 1.6 K. The measurements were performed in a perpendicular magnetic field and for different tilt angles Θ using *in situ* rotation of the sample.

Figure 3 shows the longitudinal and Hall resistivities as a function of magnetic field for (a) a 500 Å wide parabolic $Al_xGa_{1-x}As$ well and (b) a 240 Å wide square GaAs well (continuous lines). We can see the complex structure of the magnetoresistance peaks as a function of B. For example, at filling factor $\nu=6$, the magnetoresistance shows an anomalous spike for both samples, which is also visible at higher filling factors. In case (b), this anomalous peak is almost ten times narrower than the two adjacent LL magnetoresistance peaks. It is worth emphasizing here that the measurements of the square well were performed at $T=1.6$ K and, therefore, the Landau levels are temperature broadened. As a consequence, the anomalous peaks are not due to the temperature broadening. For the case of Fig. 3(a), the energy scales are smaller, and we are not able to see such a dramatic difference, since the energy gap at filling factor $\nu=6$ collapses as temperature increases. In this case, the anomalous peak at $\nu=6$ is only about 2.5 times narrower than the peak at $\nu=4.5$. We attribute such spike to the Landau-level crossing

TABLE I. Sample parameters: W is the thickness of the well; n_+ is the effective bulk density of the parabolic wells; n_s is the electron density; E_2-E_1 and $E_2^*-E_1^*$ are the subband separation energies determined from the position of the ring structure and self-consistent calculations, respectively; W_{eff} is the effective thickness of the electronic slab, μ is the zero-field mobility. α is the coefficient determined from the exchange energy (see the text).

Sample	Spacer (Å)	Well shape	W (Å)	n^+ (10^{16} cm^{-3})	n_s (10^{11} cm^{-2})	E_2-E_1 (meV)	$E_2^*-E_1^*$ (meV)	W_{eff} (Å)	μ (cm^2/V s)	α
3217	250	Square	240		8.0	23	17.2	240	594700	0.07
2537	250	Parabolic	500	47.6	4.4	14.2	14.7	92.4	590000	0.07
2536	250	Parabolic	750	21	4.4	10	8	210	322000	0.07

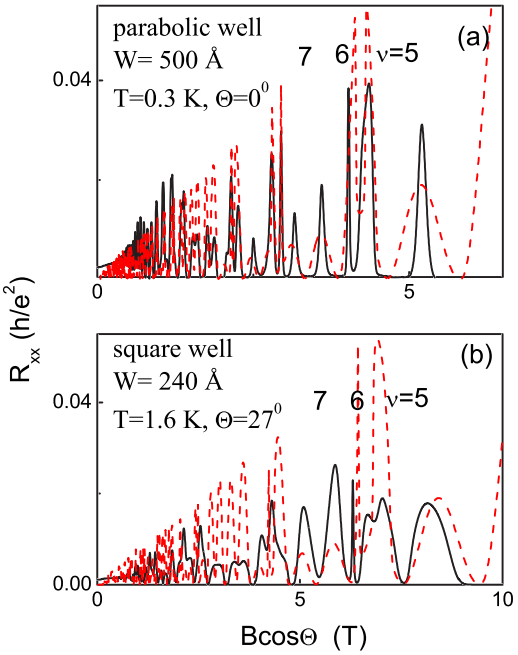

FIG. 3. (Color online) Magnetoresistances of (a) a 500 Å wide $Al_xGa_{1-x}As$ parabolic and (b) a 240 Å wide square GaAs well as a function of the perpendicular magnetic field. The dashed curves are calculated resistances from the noninteracting two-subband model (see the text). Filling factors measured from the Hall resistance are labeled.

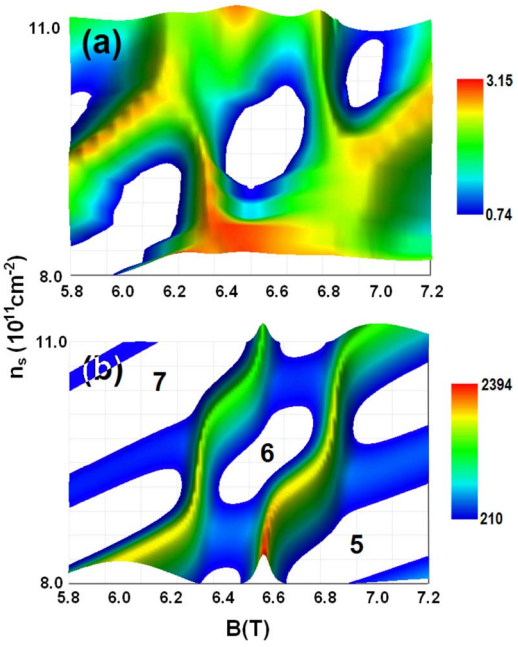

FIG. 4. (Color online) Experimentally determined plot of the (a) longitudinal resistivity at $T=1.5$ K and (b) calculated resistivity in the n_s-B plane for a 240 Å square GaAs well. Filling factors measured from the Hall resistance are labeled.

point in the Landau-level fan diagram. Naively, we may expect the vanishing of the quantum Hall minima in the LL coincident point for a single-particle picture or some modification of the energy gap due to interlevel anticrossing effect due to electron-electron interaction. Below, we demonstrate that the noninteracting model describes the entire magnetoresistance structure, including the spikes, and its dependence on the density and tilt angle.

The carrier density in the samples was varied by applying a gate voltage in order to produce the n_s-B phase diagrams in a perpendicular magnetic field. Numerous scans were taken by fixing the density and sweeping the magnetic field, producing the color map plots of the magnetoresistivity, as shown in Figs. 2(c) and 4(a).

These diagrams clearly show ringlike structures similar to the ones observed by Zhang *et al.* in a square quantum well.[3] We also found these structures in the phase diagram of the Hall resistance (not shown). At the four different crossing points labeled as A, B, C, and D in Figs. 2(a)–2(c), the LL with the following quantum numbers are involved: total filling factor $\nu_{tot}=5$: (0,2,↑) and (1,0,↑); total filling factor $\nu_{tot}=6$ at lower field: (0,2,↓) and (1,0,↑); total filling factor $\nu_{tot}=6$ at high field: (0,2,↑) and (1,0,↓); total filling factor $\nu_{tot}=7$: (0,2,↓) and (1,0,↓). In the magnetoresistance n_s-B diagrams, the regions around such LL crossing points are characterized by stripes that cross resistance minima at corresponding filling factors. For example, in Fig. 2(b), the stripe around point A crosses the resistance minimum at filling factor 6; the stripe around point B crosses the minimum at filling factor 5, and so on. These stripes appear in magnetoresistance curves as the above mentioned spikes (as in Fig. 3). The narrowing and the disappearance of the "anomalous" spikes in the level-crossing regime (which appear at filling factor 6 in Fig. 3) may serve as a precursor of the quantum Hall ferromagnet transitions.

As has been indicated in Ref. 6 (see also earlier analysis in bilayer systems[8]), the Landau-level fan diagram cannot be directly mapped by the n_s-B topological diagram produced from the magnetoresistance measurements. This reflects the fact that only the electrons from the Fermi level contribute to the conductivity, and on the other side, the Fermi energy strongly oscillates with the magnetic field. The mapping of the magnetoresistance requires exact knowledge of the density of states (DOS) of the two-dimensional electron gas (2DEG) in a strong magnetic field. To generate the conductivities, and hence the resistivities, we adopted the Lorentzian form of the density of states for the magnetoresistance calculations in a strong magnetic field.[4] Oscillations of the Fermi energy are calculated from the equation (in the ideal zero-temperature case)

$$n_s = \int_{-\infty}^{E_F(B)} \mathrm{DOS}(B,E)dE, \tag{1}$$

where DOS (B,E) is the density of states. We may approximate the density of states by a sum of Lorentzians centered on each Landau level $E_N=\hbar\omega_c\left(N+\frac{1}{2}\right)$, where $\omega_c=\frac{eB}{m^*}$ is the cyclotron frequency. The DOS is given by (including spin and subband indices s,i)

$$\mathrm{DOS}(E,B) = \frac{eB}{h}\sum_{N=0}^{\infty}\sum_{i=0,1}\sum_{s=+,-}\frac{\Gamma}{1+\left(\frac{E_{N,i,s}-E}{\Gamma}\right)^2}. \quad (2)$$

The longitudinal conductivity σ_{xx} was calculated by

$$\sigma_{xx}(B) = \frac{e^2}{h}\sum_{N=0}^{\infty}\sum_{i=0,1}\sum_{s=+,-}\left(N+\frac{1}{2}\right)\frac{1}{1+2\left(\frac{E_{N,i,s}-E_F(B)}{\Gamma}\right)^2}, \quad (3)$$

where the energy levels associated with the hybrid subband energies in the tilted fields E_α and E_β (they will be defined in the next section) are

$$E_{N,0,s} = \left(N+\frac{1}{2}\right)E_\alpha + s\frac{1}{2}g^*\mu_B B, \quad (4)$$

$$E_{N,1,s} = \left(N+\frac{1}{2}\right)E_\alpha + E_\beta + s\frac{1}{2}g^*\mu_B B. \quad (5)$$

In our calculations, we used a level broadening $\Gamma=\hbar/\tau_q$ independent of the magnetic field. Making this choice, we found a better agreement with the experimental data rather than using a magnetic field dependent level broadening like the square-root dependence in the case of the self-consistent Born approximation. In fact, many other authors have found different dependencies[9] and, as pointed out by Raikh and Shahbazyan,[10] when the correlation length is larger than the Larmor radius, the broadening is independent of the magnetic field, and this condition is verified in the region of high magnetic fields. The correlation length is not properly known, but the condition above is very likely to occur in our samples because, in high magnetic fields, the Larmor radius is smaller than the potential correlation length. The fitted value $\Gamma=0.066$ meV is about ten times smaller than the one obtained from the amplitude of the Shubnikov–de Haas oscillations in a low magnetic field. We attribute this difference to the fact that, in our approximation, we did not consider the delocalized states.[11]

It is worth noting that the factor g^* includes the bare contribution g_0 due to the Zeeman energy which depends on the total magnetic field B, and an exchange contribution E_{ex} which depends only on the perpendicular component of the field $B_\perp$. The total contribution can be written as[12,13]

$$g^*\mu_B B = g_0\mu_B B + E_{\mathrm{ex}}(B_\perp), \quad (6)$$

where μ_B is the Bohr magneton and $E_{\mathrm{ex}}=\alpha\hbar\omega_c$.

The longitudinal resistivity ρ_{xx} was calculated as a function of the longitudinal and Hall conductivities σ_{xx} and σ_{xy} by simply using the Drude formula $\rho_{xx}=\sigma_{xx}/(\sigma_{xx}^2+\sigma_{xy}^2)$, where the Hall conductivity is given by $\sigma_{xy}=n_s e/B_{\mathrm{bot}}$

An experimental n_s-B plot that corresponds to the above figures is shown in Fig. 2(c). This figure presents the result of the measurements in an $Al_xGa_{1-x}As$ parabolic quantum well 500 Å wide at the temperature $T=50$ mK. We can see the similarity between Figs. 2(b) and 2(c). Note that the range of values of n_s in Fig. 2(c) goes from 4.9×10^{11} to 6.8×10^{11} cm^{-2}.

The calculated magnetoresistances ρ_{xx} are presented in Fig. 3 (dashed lines) and reproduce the position of all the spikes. Since the localization effects were not included in our model, the peak broadening of the simulated curves at low temperatures [Fig. 3(a)] is significantly larger than for the experimental data. However, at high temperatures [Fig. 3(b)], we can see a resemblance between the theoretical and experimental traces. The similarities demonstrate that this simple model contains the essential physics necessary to account for the peak broadening and their position. For example, at filling factor $\nu=6$ in Fig. 3, we may see narrow spikes, which in other systems have been identified with magnetic transition between the two Ising-like states in the QHF at the LL crossing due to their anomalous width and magnetic field position.[5,20] In the noninteracting model, such spikes originate from the nonmonotonic behavior of the Fermi energy with magnetic field. Due to magnetic quantization, the Fermi energy is pinned by the Landau levels and makes discrete jumps as a function of field in order to be close to the value of the Fermi energy at zero field. If only one electron subband is occupied, the calculated magnetoresistance shows the Shubnikov–de Haas spectrum, which consists of broad peaks and narrow minima, which agrees with high temperature measurements of R_{xx} in high mobility samples. We should note that the broadening of the magnetoresistance peaks in strong magnetic fields is determined by the pinning of the Fermi level, not by the LL broadening due to the scattering. If two subbands are occupied, the Fermi level is not pinned in the LL coincident point and abruptly falls from pseudospin up into a pseudospin down state. The width of the peaks in R_{xx} in LL coincident points are determined by LL broadening, which is ten times smaller than the effective broadening of the peaks far from the crossing points. If the temperature falls down, the states in the band tails of each LL are localized, and all magnetoresistance peaks become narrow.

We calculated ρ_{xx} for different densities as a function of magnetic field and produced the topological diagrams shown in Figs. 2(b) and 4(b). From the comparison of the position of the center of the rings, we deduced the subband separation energies E_1-E_0 which are shown in Table I. From the comparison of the size of the rings, we determined the correlation energies E_{ex} and, consequently, the parameter α. We found that the value of α was two to three times smaller than the one determined from the spin-splitting collapse in single subband samples.[12,14] Aleiner and Glazman[15] predicted a weak dependence of the parameter α on the electron density $\alpha=(1/\pi k_F a_B)\ln(2k_F a_B)$, yielding a value $\alpha=0.21-0.22$ for our structures. Such discrepancy may indicate that different physical effects are involved in the spin collapse and LL crossing regimes. The calculation of the corresponding magnetoresistivity map in the n_s-B plane in the same range of values of magnetic field gives the diagram shown in Fig. 2(b). In this diagram, we choose a range of electron concentration in order to see the peculiar structure seen in the figure (from 4.5. to 7.5×10^{11} cm^{-2}). This structure does not resemble the diamond of Fig. 2(a) and is a more complex structure that resembles a deformed ring. After an inspection, we may identify the filling factors in each region of the diagram, which are shown in the figure. We marked in Figs. 2(a)

and 2(b) the points labeled as A, B, C, and D, which correspond with each other in both figures. We can deduce that the diamond in Fig. 2(a) corresponds directly to the ring in Fig. 2(b). In fact, the topological ringlike structures can be easily identified with the diamond structures in the LL fan diagram of a two-subband system at the locations of the LL crossings.[3,5] To understand the relationship between both structures, let us follow the level (1,0,↑) in Fig. 2(a), starting from $B=3.5$ T, where its energy is around 17.0 meV. At this point, it crosses the Fermi energy corresponding to $n_s=5.6\times10^{11}$ cm^{-2}. By increasing the magnetic field, the same Landau level crosses Fermi energies corresponding to different values of n_s. From 3.5 T to approximately 3.8 T, n_s increases up to about 6.0×10^{11} cm^{-2}. Above this field, the level crosses Fermi energies corresponding to decreasing values of n_s and in point A, this level crosses the level (0,2,↓) (at $B=3.88$ T). The same picture is verified in Fig. 2(b). In this figure, the stripe that starts at 5.6×10^{11} cm^{-2} at $B=3.5$ T corresponds exactly to the Landau level (1,0,↑). By increasing the magnetic field, this stripe initially moves up to higher n_s values and at around $B=3.8$ T starts to move down to lower values of n_s. At point A, this stripe crosses another stripe that started at $B=3.5$ T with $n_s\approx4.8\times10^{11}$ cm^{-2}. A careful inspection reveals the direct correspondence between Figs. 2(a) and 2(b) and common points A, B, C, and D, as mentioned. In other words, the diamondlike structure in the Landau fan diagram is mapped into the ring structure by means of the nonmonotonicity of the Fermi energy with respect to the magnetic field.

III. EXPERIMENTAL RESULTS IN A TILTED MAGNETIC FIELD

In general, there is no difference in LL crossing physics when we investigate the n_s or tilt angle dependence of the magnetoresistance. However, the tilted field method may provide additional and independent information about interaction-induced gaps and the Fermi-level trajectory in the quantum Hall effect regime. Therefore, it is useful to check the topological features of the phase diagram in the Θ-B plane and compare them with a simple model. In order to do it, we measured the magnetoresistance in a tilted magnetic field by rotating our samples *in situ*. We built tilt angle–magnetic field phase diagrams for different densities and wells. Figures 5(a) and 6(a) show the magnetoresistivity plots as a function of the perpendicular component of the magnetic field for the 500 Å wide parabolic and the 240 Å wide square quantum wells for fixed densities. We can clearly see the set of the LL crossing points in these diagrams. In both figures, there is a set of vertical lines accompanied by arches which turn right, crossing regions of minimum resistance. It is interesting to check if we can reproduce such topological features of the phase diagrams from the model discussed above. We start from the formalism[16] where the energy eigenvalues of the Hamiltonian for a harmonic potential in a tilted magnetic field have been derived analytically. The resulting energies are $(n_\alpha+1/2)E_\alpha+(n_\beta+1/2)E_\beta$ in terms of the positive integer quantum numbers n_α and n_β, and the two energies $E_\alpha(B)$ and $E_\beta(B)$ are given by

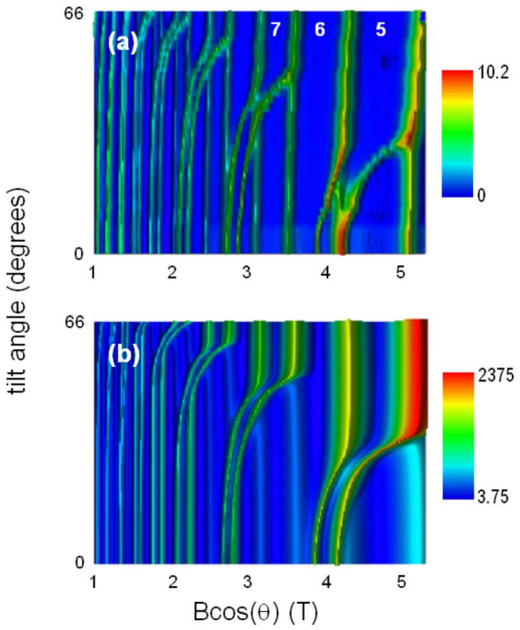

FIG. 5. (Color online) Experimentally determined plot of the (a) longitudinal resistivity at $T=300$ mK and (b) calculated resistivity in the Θ-B plane for a 500 Å $Al_xGa_{1-x}As$ parabolic well. Filling factors measured from the Hall resistance are labeled.

$$E_\alpha(B)=\hbar(\omega_c^2\cos^2(\phi)+\Omega^2\sin^2(\phi)-\omega_c\Omega\sin(2\phi)\sin(\theta))^{1/2}, \tag{7}$$

$$E_\beta(B)=\hbar(\omega_c^2\sin^2(\phi)+\Omega^2\cos^2(\phi)+\omega_c\Omega\sin(2\phi)\sin(\theta))^{1/2}, \tag{8}$$

where θ is the tilt angle and ϕ is an angle defined by the expression $\tan(2\phi)=\frac{2\omega_c\Omega\sin(\theta)}{(\Omega^2-\omega_c^2)}$. The parameter Ω is associated to the conduction-band parabolic potential along the z direction, which is given by $\frac{1}{2}m^*\Omega^2z^2$. The electron-electron interaction in the quantum well changes the bare harmonic potential in some way, but in a first approximation, the overall shape may be considered almost parabolic in our parabolic-well samples with an effective Ω different from that of the empty-well case, Ω_0. The value of Ω is obtained by the best fit of the experimental curves to the theoretical model.

For a perpendicular magnetic field, n_α is identical to the Landau-level index N and n_β is associated to the subband index, so that the subband energy separation is given by $E_\beta\equiv\hbar\Omega=E_1-E_0$ and $E_\alpha=\hbar\omega_c$. However, in a tilted field, we should substitute the energies in Eqs. (4) and (5) by E_α and E_β from Eqs. (7) and (8).

The calculated Θ-B phase diagrams for our square and parabolic wells are presented in Figs. 5(b) and 6(b). As can be seen, they show similarities with Figs. 5(a) and 6(a), which indicates that this simple model contains the essential physics behind the LL crossing regime. We can see that the model reproduces all the key features in the phase-diagram topology, as well as the position of the LL degeneracy regions. It is worth noting that, for a square quantum well, the

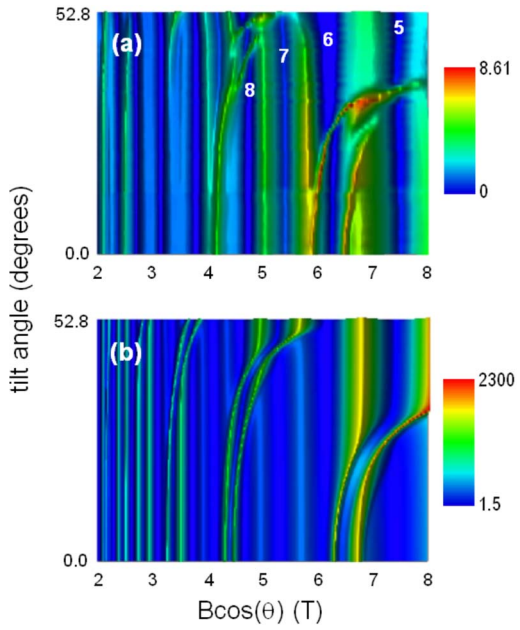

FIG. 6. (Color online) Experimentally determined plot of the (a) longitudinal resistivity at $T=1.6$ K and (b) calculated resistivity in the Θ-B plane for a 240 Å square GaAs well. Filling factors measured from the Hall resistance are labeled.

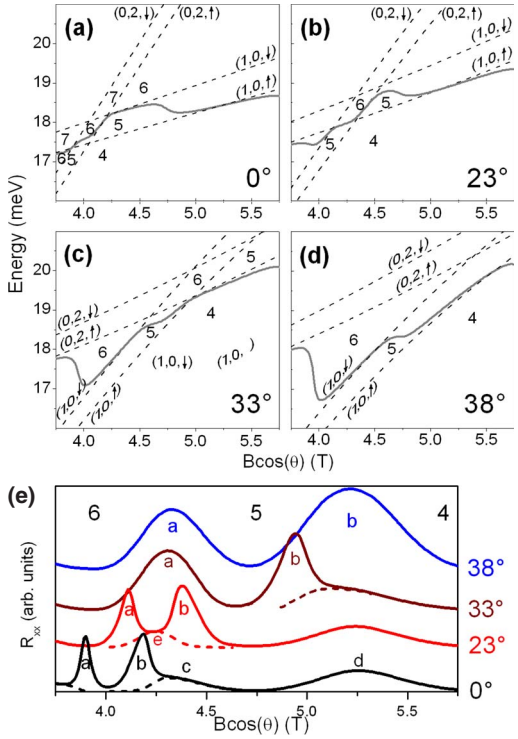

FIG. 7. (Color online) Details of the Landau fans for different tilt angles from $B=3.75$ T to $B=5.75$ mT showing the crossing of levels presented also in Fig. 1 (here, some filling factors are shown): (a) tilt angle of 0°, (b) tilt angle of 23°, (c) tilt angle of 33°, and (d) tilt angle of 38°. In these figures, the dashed lines are Landau levels (spin splitted) and the winding gray lines are the Fermi levels. In (e), we present the magnetoresistances corresponding to the same angles (indicated at the right). The position of the filling factors 4, 5, and 6 is also shown.

discrepancy between theory and experiment can be explained by the deficiency of the model.[16] For example, the energy spacing in the harmonic potential is proportional to $\cos\Theta$, while in the square well, a $\cos^2\Theta$ dependence is expected[17] in the limit of a strong magnetic field. It explains the shift of the center of the structure of arches in Fig. 6(a) at filling factor $\nu=8$ to higher Θ in comparison with Fig. 6(b).

To better understand these diagrams, we show in Fig. 7 the Landau fans corresponding to the plot of Fig. 5(b) for different tilt angles [(a) 0°, (b) 23°, (c) 33°, and (d) 38°] from $B=3.75$ T to $B=5.75$ T. In Fig. 7(e), we present the corresponding magnetoresistance curves. The crossing of levels at a perpendicular magnetic field shown in Fig. 7(a) reproduces the panorama of Fig. 1. As the tilt angle is increased, the diamond centered at filling factor 6 [centered at ~4.0 T in Fig. 7(a)] moves right and up, and at 38°, it is almost hidden. In Fig. 7(a), the Fermi level [thick winding gray lines in Figs. 7(a)–7(d)] passes inside the diamond, which gives a minimum in the magnetoresistance. In fact, in Fig. 7(e) (curve for 0°), this minimum is located between peaks *a* and *b*, which correspond to the levels (0,2,↓) and (0,2,↑) respectively. On the other side, the very wide and low peaks of magnetoresistance centered at ~4.3 T (peak *c*) and ~5.25 T (peak *d*) correspond to the passage of the Fermi level in levels (1,0,↓) and (1,0,↑). At the tilt angle of 23° [Fig. 7(b)], the Fermi level passes on the lower boundary of the diamond that divides regions of filling factors 5 and 6. This leads to the appearance of a peak centered at ~4.25 T labeled *e* [see the corresponding magnetoresistance curve in Fig. 7(e)], and peaks *a* and *b* have displaced further to the right, accompanying the movement of the diamond. However, at this angle, the Fermi level does not yet pass on level (1,0,↓). This causes the disappearance of peak *c* that was seen at 0°. This shows that peaks *c* and *e* have distinct origins. Now, in Fig. 7(c) (angle of 33°), the Fermi level passes below the diamond, crossing the region of filling factor 5. At this moment, peak *e* disappeared; peaks *a* and *b* have moved again to the right. Finally, at the angle of 38° [Fig. 7(d)] and above, peak *d* disappeared as the Fermi level does not yet cross the level (0,2,↑), and the feature centered at ~5.25 T corresponds uniquely to peak *b*. The Fermi level crosses only the levels (1,0,↓) and (1,0,↑), and the levels (2,0,↓,↑) are definitively depopulated in this threshold angle. The arches seen in the plots of Fig. 5 in the same range of magnetic field correspond, consequently, to peaks *a* and *b*. At angles above ~35°, these peaks remain fixed in the magnetic field axis so that the arches end, giving place to vertical lines. We infer that the appearance of arches in both Figs. 5 and 6 is a consequence of two-subband occupancy, and the threshold of the disappearance of any pair of arches is associated to the depopulation of a particular Landau level of the second subband.

Finally, it is worth noting that the topological diagrams in the Θ-B plane obtained in this paper for narrow parabolic and square wells are very different from the diagrams which have been measured in 2000–3000 Å wide parabolic wells in Ref. 7. For example, Figs. 5 and 6 show shifts of the position of the peaks in the shape of arches from high to low

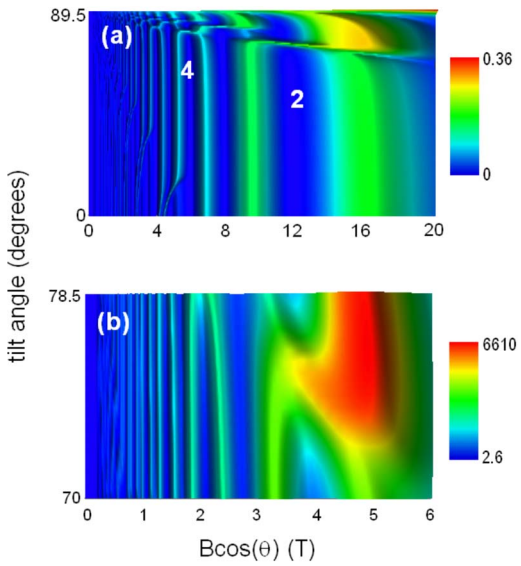

FIG. 8. (Color online) Calculated resistivity in the Θ-B plane for (a) a 500 Å and (b) a 2000 Å wide $Al_xGa_{1-x}As$ parabolic well. The calculations are extended to higher magnetic field and larger tilt angles. The figures display the features associated with the LL coincidence for opposite spin and different Landau orbital indices within the same subband. For reference, in (a), the filling factors 2 and 4 are labeled.

filling factor ν with increasing tilt angle. This observation disagrees with the behavior of the anomalous peak in the magnetoresistance traces of the 2000 Å wide parabolic well, which is shifted in the opposite direction with Θ (see Fig. 5 in Ref. 7). Such a behavior can be explained by the different character of the LL crossing. In the 2000 Å wide parabolic well, the second subband is depopulated at low magnetic field and, therefore, the alignment of the two LL with opposite spin and different Landau orbital indices should be expected within the same subband. Note that for wide wells, LL crossing can occur at small tilt angle, since the two-dimensional Landau states collapse into the three-dimensional Landau bands,[18] which contributes to decrease of the energy E_α with Θ. For narrow GaAs wells and single $Al_xGa_{1-x}As$ heterostructures, LL crossing occurs because the bare Zeeman splitting, which is proportional to the total magnetic field ($\sim B_{tot}$), can be larger than the cyclotron energy which is proportional to the perpendicular component of the magnetic field ($\sim B_\perp$). In Figure 8(a), we plot the calculated Θ-$B_\perp$ topological diagram for the 500 Å wide parabolic $Al_xGa_{1-x}As$ well, which we extended to higher magnetic field and tilt angle. We can observe lines crossing the filling factors 2 and 4 with negative slopes, while in Figs. 5 and 6, the crossing lines have positive slopes. We attribute the magnetoresistance peak at filling factor $\nu=2$ to the coincidence between the $(0,1,\uparrow)$ and $(0,0,\downarrow)$ levels. Figure 8(b) displays the calculated Θ-$B_\perp$ topological diagram for the 2000 Å wide parabolic $Al_xGa_{1-x}As$ well in order to allow a comparison with our early study of the LL crossing in wide parabolic wells.[7] We can see that the simple simulations of the Θ-$B_\perp$ phase-diagram topology is in good agreement with the experiment (Fig. 5 in Ref. 7).

We would like to complete this work with a short discussion of the previous study of the LL crossing regime and our observations. As we mentioned above, although substantial progress has been made in understanding the quantum Hall ferromagnetism, the theoretical and experimental results remain controversial. Theory predicts the emergence of interaction-driven gaps when the interaction energy competes with the disorder energy.[2] Therefore, the spikes in the magnetoresistance minima at even filling factors due to the Fermi energy locking at the crossing points (see Fig. 1) should disappear.[4] On the other hand, the fluctuations of the potential results in domain formation that introduces the additional domain-wall scattering, which leads to the spikes in the quantum Hall minima.[19,20] In the present paper, we report the observation of spikes in the GaAs/AlGaAs system and explain them in terms of the nonmonotonic behavior of the Fermi energy in the cross-level regime within the simple single-particle model. The disappearance of the spikes at high magnetic field[4] can be explained by the inhomogeneity of the density in the realistic sample, which becomes more important in a strong field, since the magnetic length decreases with B. Surely, more detailed and careful analysis of the magnetoresistance behavior in the LL crossing regime is necessary in order to distinguish between QHF and a simple-level coincidence effect.

In conclusion, we performed detailed measurements of the magnetoresistance in parabolic $Al_xGa_{1-x}As$ and square GaAs quantum wells with two occupied subbands as a function of the density and tilt angle. We built the topological diagrams in the n_s-$B_\perp$ and Θ-$B_\perp$ planes and compared them with simulations based on a single-particle harmonic potential approximation. The variation of the tilt angle leads to a complex structure of superposition of magnetoresistance peaks, which depends intrinsically on the oscillations of the Fermi level as a function of magnetic field.

ACKNOWLEDGMENTS

Support of this work by FAPESP and CNPq (Brazilian funding agencies) is acknowledged.

*Present address: Institute of Semiconductor Physics, Novosibirst 630090, Russia.

[1] G. M. Girvin, Phys. Today **53**(6), 39 (2000).
[2] T. Jungwirth and A. H. MacDonald, Phys. Rev. B **63**, 035305 (2000).
[3] X. C. Zhang, D. R. Faulhaber, and H. W. Jiang, Phys. Rev. Lett. **95**, 216801 (2005).
[4] X. C. Zhang, I. Martin, and H. W. Jiang, Phys. Rev. B **74**, 073301 (2006).
[5] K. Muraki, T. Saku, and Y. Hirayama, Phys. Rev. Lett. **87**,

196801 (2001).
[6] C. Ellenberger, B. Simovič, R. Letureq, T. Ihn, S. E. Ulloa, K. Ensslin, D. C. Driscoll, and A. C. Gossard, Phys. Rev. B **74**, 195313 (2006).
[7] G. M. Gusev, A. A. Quivy, T. E. Lamas, J. R. Leite, O. Estibals, and J. C. Portal, Phys. Rev. B **67**, 155313 (2003).
[8] A. G. Davies, C. H. W. Barnes, K. R. Zolleis, J. T. Nicholls, M. Y. Simmons, and D. A. Ritchie, Phys. Rev. B **54**, R17331 (1996).
[9] E. Gornik, R. Lassnig, G. Strasser, H. L. Störmer, A. C. Gossard, and W. Wiegmann, Phys. Rev. Lett. **54**, 1820 (1985); J. K. Wang, J. H. Campbell, D. C. Tsui, and A. Y. Cho, Phys. Rev. B **38**, 6174 (1988); T. P. Smith, B. B. Goldberg, P. J. Stiles, and M. Heiblum, *ibid.* **32**, 2696 (1985).
[10] M. E. Raikh and T. V. Shahbazyan, Phys. Rev. B **47**, 1522 (1993).
[11] G. Gobsch, D. Schulze, and G. Paasch, Phys. Rev. B **38**, 10943 (1988).
[12] D. R. Leadley, R. J. Nicholas, J. J. Harris, and C. T. Foxon, Phys. Rev. B **58**, 13036 (1998).
[13] M. M. Fogler and B. I. Shklovskii, Phys. Rev. B **52**, 17366 (1995).
[14] C. A. Duarte, G. M. Gusev, A. A. Quivy, T. E. Lamas, and J. C. Portal, Physica E (Amsterdam) **34**, 488 (2006).
[15] I. L. Aleiner and L. I. Glazman, Phys. Rev. B **52**, 11296 (1995).
[16] R. Merlin, Solid State Commun. **64**, 99 (1987).
[17] C. S. Sergio, G. M. Gusev, A. A. Quivy, T. E. Lamas, J. R. Leite, O. Estibals, and J. C. Portal, Microelectron. J. **34**, 763 (2003).
[18] G. M. Gusev, A. A. Quivy, T. E. Lamas, J. R. Leite, A. K. Bakarov, A. I. Toropov, O. Estibals, and J. C. Portal, Phys. Rev. B **65**, 205316 (2002).
[19] T. Jungwirth and A. H. MacDonald, Phys. Rev. Lett. **87**, 216801 (2001).
[20] E. P. Poortere, E. Tutuk, S. J. Papadakis, and M. Shayegan, Science **290**, 1546 (2000).